

Supporting Information

Segmental, Domain-Selective Perdeuteration and Small-Angle Neutron Scattering for Structural Analysis of Multi-Domain Proteins

Miriam Sonntag⁺, Pravin Kumar Ankush Jagtap⁺, Bernd Simon, Marie-Sousai Appavou, Arie Geerlof, Ralf Stehle, Frank Gabel, Janosch Hennig, and Michael Sattler**

anie_201702904_sm_miscellaneous_information.pdf

SUPPORTING INFORMATION

Table of Contents

Material and Methods	S3-4
Figure S1. Overlay of ^1H , ^{15}N HSQC NMR spectra of different TIA-1 constructs	S5
Figure S2. Quality assessment of all three constructs	S6
Figure S3. Assessment of the deuteration level of segmentally labeled protein samples	S7
Figure S4. Scattering densities as a function of D_2O concentration in aqueous solvents	S7
Figure S5. Solution NMR structure of TIA-1 RRM1	S8
Figure S6. Structure analysis of TIA-1 RRM1	S8
Figure S7. Crystal structure of TIA-1 RRM2 in complex with RNA	S9
Figure S8. Conformation space and statistics of structure calculations	S9
Table S1. Small-angle X-ray scattering statistic	S10
Table S2. Small-angle neutron scattering statistic	S11
Table S3. Structural statistics for TIA-1 RRM1	S12
Table S4. Crystal structure statistics for TIA-1 RRM2 in complex with RNA	S13
Table S5 Statistics of structure calculations for TIA-1 RRM123	S14
References	S15

SUPPORTING INFORMATION

Material and Methods

Plasmids, protein expression, purification and sample preparation

Plasmids for TIA-1 wildtype, sortase A, RRM1 and RRM23 for sortase ligation, RRM23 (93-274) for crystallization and RRM1 (1-92) for NMR structure determination were derived from pET-24d (+) (Merck/Novagen) and contain an N-terminal His-tag, a thioredoxin fusion tag and a TEV protease cleavage site. Both RRM1 constructs for sortase ligation contained an additional C-terminal His-tag. The constructs for sortase ligation were designed, expressed and purified as previously described.^[1] Wild type TIA-1 was expressed and purified according to the same protocol. Proteins for crystallization and small-angle X-ray scattering (SAXS) were expressed in LB medium, whereas proteins for NMR spectroscopy and small-angle neutron scattering (SANS) were expressed in differently isotope labeled M9 minimal medium. For NMR experiments the M9 media was supplemented with either ¹³C glucose and/or ¹⁵N NH₄Cl. For SANS measurements, we used ²H glucose and dissolved all waterfree M9 salts, trace elements, biotin, thiamin, IPTG, CaCl₂, and MgSO₄ in 99.8 % D₂O (all isotopes were purchased from Sigma). Coomassie stained SDS gel electrophoresis assessed protein quality.

NMR spectroscopy

NMR ¹H, ¹⁵N HSQC experiments were carried out at 298 K on an 800 MHz Bruker Avance III spectrometer. NMR experiments were processed with NMRPipe^[2] and analyzed with SPARKY.^[3] Samples contained 0.05 mM protein in 10 mM potassium phosphate pH 6.0, 50 mM NaCl, 1 mM 2-mercaptoethanol and 10 % D₂O added for the lock.

NMR spectra for RRM1 structure calculation were acquired at 298 K using a AVIII500, AVIII600, AVIII750, AVIII800 and a AVI900 Bruker NMR spectrometer, equipped with cryogenic or room temperature (750 MHz) triple resonance gradient probes. Sample contained ~0.5 mM TIA-1 RRM1 protein in 50 mM Potassium phosphate (pH 6.0), 100 mM NaCl, 1 mM DTT with 10 % D₂O added for the lock. All spectra were processed using NMRPipe/Draw^[2] and analyzed using NMRView^[4] software. Protein backbone assignments for ¹⁵N, ¹HN, ¹³C_α, ¹³C_β, and ¹³C' chemical shifts were obtained from HNCA, HNCACB, CBCA(CO)NH and HNCOC experiments^[5] and assignments were made manually in CARA^[6] software. Three-dimensional total correlation spectroscopy (TOCSY) experiments were performed to assign carbon and proton resonances of the RRM1 side chains. Two HCCH-TOCSY experiments with ¹³C and ¹H evolution were recorded for this, along with CC(CO)NH-TOCSY and HBHA(CO)NH^[7] experiments to correlate the amide group resonances with the side-chain residues. Aromatic resonances were assigned using 2-D ¹H-¹³C HSQC, HBCBCGCDHD, HBCBCGCDCEHE^[8] and ¹³C edited NOESY-HSQC spectra. Assignment of side-chain residues and picking of NOESY cross-peaks was carried out in CCPN analysis^[9] software.

The NMR structure of TIA-1 RRM1 domain was calculated using CYANA 3.0^[10]. The NOESY cross-peaks in ¹⁵N- and ¹³C-edited NOESY-HSQC spectra were assigned in an automated way using CYANA 3.0 and subsequently checked manually. Dihedral angle restraints were predicted using TALOS+.^[11] 200 structures were calculated using these restraints and the structures were further refined using explicit solvent in ARIA 1.2.^[12] An ensemble of 20 lowest energy structures were selected and further used for structure validation by iCing^[13], PROCHECK^[14] and WHATCHECK.^[15]

Small-angle neutron scattering

All samples (including water and buffers) were measured in Hellma 110-QX quartz cuvettes with 1 mm optical path length at the large dynamic range diffractometers KWS-1 and KWS-2 at the Heinz Maier-Leibnitz Zentrum.^[16] Scattering data of all samples were recorded at two different detector distances (2 m and 8 m) at a neutron wavelength of $\lambda = 4.55$ and 4.72 Å for KWS-2 and KWS-1 respectively, resulting in a Q range of 0.0007-0.5 Å⁻¹. Measurements were carried out at 298 K. H₂O/D₂O buffers, an empty quartz cuvette, the empty beam, a Plexiglas sample as well as a boron carbide sample were measured for data reduction. Exposure times varied between 10-15 min at 2 m detector distance and 90-120 min at 8 m detector distance. Transmission was measured for 1 min at 4 m detector distance for all samples and the empty beam using the direct beam. 200 µl samples contained 5 mg/ml protein in 10 mM potassium phosphate pH 6.0, 50 mM NaCl and 10 mM DTT with different D₂O concentrations (0 % and 42 %). For the RNA bound samples, 1.05 equivalents of U15 oligonucleotides (synthesized, IBA GmbH) were added to the protein.

SANS data reduction

Data treatment and visualization of above mentioned neutron scattering measurements have been performed using the freely available software QtiKWS. The data were collected on a 2D detector and radially averaged in order to obtain 1D intensity patterns. The recorded data were corrected for instrumental background with a boron carbide sample, for transmission and for detector sensitivity determined by a measurement of a 1.5 mm-thick polymethylmethacrylate (Plexiglas®). Absolute calibration of scattering cross sections $d\Sigma/d\Omega(q)$ per unit sample volume in cm⁻¹ was obtained thanks to a calibration with the Plexiglas® sample. For all samples the empty cuvette and the respective solvent (deuterated or mixture of deuterated and protonated buffer) was measured as reference and subtracted from the corrected data.

SUPPORTING INFORMATION

Small-angle X-ray scattering

All samples and buffers were measured at 20° C on a Rigaku BIOSAXS1000 instrument with a HF007 microfocus generator equipped with a Cu-target at 40 kV and 30 mA. Transmissions were measured with a photodiode beamstop, q-calibration was done by a silver-behenate measurement. Measurements were done in eight 900-second frames checked for beam damage and averaged. Absolute calibration was done with a sample of glassy carbon which was cross calibrated with water according to Fan et al.^[17] A dilution series ranging from 1 – 5 mg/ml was measured for each protein and complex sample. For the complex samples, 1.2 equivalents of U15 RNA were added to each protein sample. Protein and complex samples were measured in 10 mM potassium phosphate pH 6.0, 50 mM NaCl and 10 mM DTT.

SAXS data reduction

Circular averaging and background subtraction was done with the Rigaku SAXSLab software v 3.0.1 r 1. The one-dimensional scattering curves expressed as a function of the modulus of the scattering vector $Q = (4\pi/\lambda)\sin\theta$ with 2θ being the scattering angle and λ being the X-ray wavelength were further analysed using the ATSAS package v 3.0.2.^[18] The radii of gyration R_g of all samples were extracted using the Guinier approximation in PRIMUS.^[19] The validity of the Guinier approximation, R_g for $Q < 1.3$, was verified and fulfilled for each sample. The pairwise distribution functions were calculated using GNOM.^[20]

Static light scattering

Static light scattering was measured at 303 K with a Malvern Viscotek instrument (TDA 305) connected downstream to an Äkta purifier equipped with an analytical size-exclusion column (Superdex 75 or 200, 10/300 GL, GE Healthcare) at 277 K. 100 μ l of each sample with 3 mg/ml was injected. As running buffer, 50 mM potassium phosphate pH 6.0, 100 mM NaCl and 1 mM 2-mercaptoethanol has been used. Elution profiles were collected for 60 min with a flow rate of 0.5 ml/min and data were collected using absorbance UV detection at 280 nm, right-angle light scattering (RALS) and refractive index (RI). The molecular weights of separated elution peaks calculated using OmniSEC software (Malvern). The detector was calibrated with a 4 mg/ml BSA solution with 66.4 kDa for the BSA monomer and dn/dc values of 0.165 and 0.185 ml/g for RNA and protein, respectively.

Structure calculations

Structures were generated using a restrained MD/SA protocol implemented in CNS.^[21] First a template structure with extended linker conformations and the high resolution structures of RRM1-3 and U15 RNA bound to RRM2 was generated. Then the N-terminus (residues 1-7) and the RRM1-2 (residues 83-97) and RRM2-3 (residues 177-195) linkers were disordered by random rotation of the Φ and Ψ backbone angles. The nucleotides U6-U10 are restraint to bind to RRM2, of which two are strictly restrained according to the distances reported in the crystal structure presented here (*vide infra*). The remaining nucleotides (U1-U5, U11-U15) are not fixed and are allowed to move freely during simulated annealing. The resulting structures were subsequently minimized by a 3-step Cartesian dynamics simulated annealing protocol^[22] with 40000 high-temperature (20000 K) steps followed by two cooling phases of 4000 steps (2000->1000K and 1000K->50K). The RRM 1-3 structures and the RRM2-RNA interface where restrained to the initial coordinates using the ncs-energy term.^[23] A pool of 5000 structures was generated and used for fitting the SANS and SAXS data using CRYSON and CRYSON (ATSAS package v 3.02 package^[18]). Figure 4a shows an ensemble of the 100 structures with the lowest CNS energy to illustrate that the pool of generated structures samples a large conformational space. Next, the pool of structures was filtered by first removing structures with coordinate clashes, by choosing a CNS-energy cut-off value at which no clashes were visible. Next we filtered out structures which fitted the SAS data within a range of χ^2 values from the lowest value observed in the pool χ^2_{\min} to a value of $1.5 \times \chi^2_{\min}$.^[24] Selection based on SAXS data recorded for the RRM-123-U15 complex (1176 structures with $0.99 < \chi^2 < 1.48$) and the RRM23-10mer complex (222 structures with $0.85 < \chi^2 < 1.27$) resulted in a total of 67 structures shown in Figure 4a. Further selecting using the SANS data in H₂O (1243 structures with $2.11 < \chi^2 < 3.16$ for H-RRM1/D-RRM23 and 727 structures with $2.00 < \chi^2 < 3.00$) reduced the ensemble to 5 structures (Fig 4a). The SANS data at 42% and 70% H₂O are not very discriminating (for D-RRM1/H-RRM23 all and for H-RRM1/D-RRM23 4398/42% and 4965/70% structures fulfill the 1.5 criterion) and thus do not lead to a further reduction of selected structures.

RRM2+RNA structure

Several crystallization screens were setup with 100 nl of 8 mg/ml RRM23 in complex with 1.2x excess of fas 10mer intron 6 RNA (UGCUUUGUUC) and 100 nl of reservoir buffer in sitting drop format. Crystals were obtained in 50 mM MES buffer pH 6.0, 5 mM magnesium sulfate, 5% PEG 4000 condition and were flash frozen in 30% glycerol mixed with reservoir solution. Datasets were collected at ID23 beam line at ESRF Grenoble, France and processed with XDS.^[25] The structure was solved by molecular replacement using Phaser^[26] from CCP4 suite^[27] and only RRM2 and two nucleotides were found in the solution likely due to the proteolytic cleavage of the protein and degradation of RNA. The structure was completed with several rounds of manual building in Coot^[28] and refinement in Refmac.^[29]

SUPPORTING INFORMATION

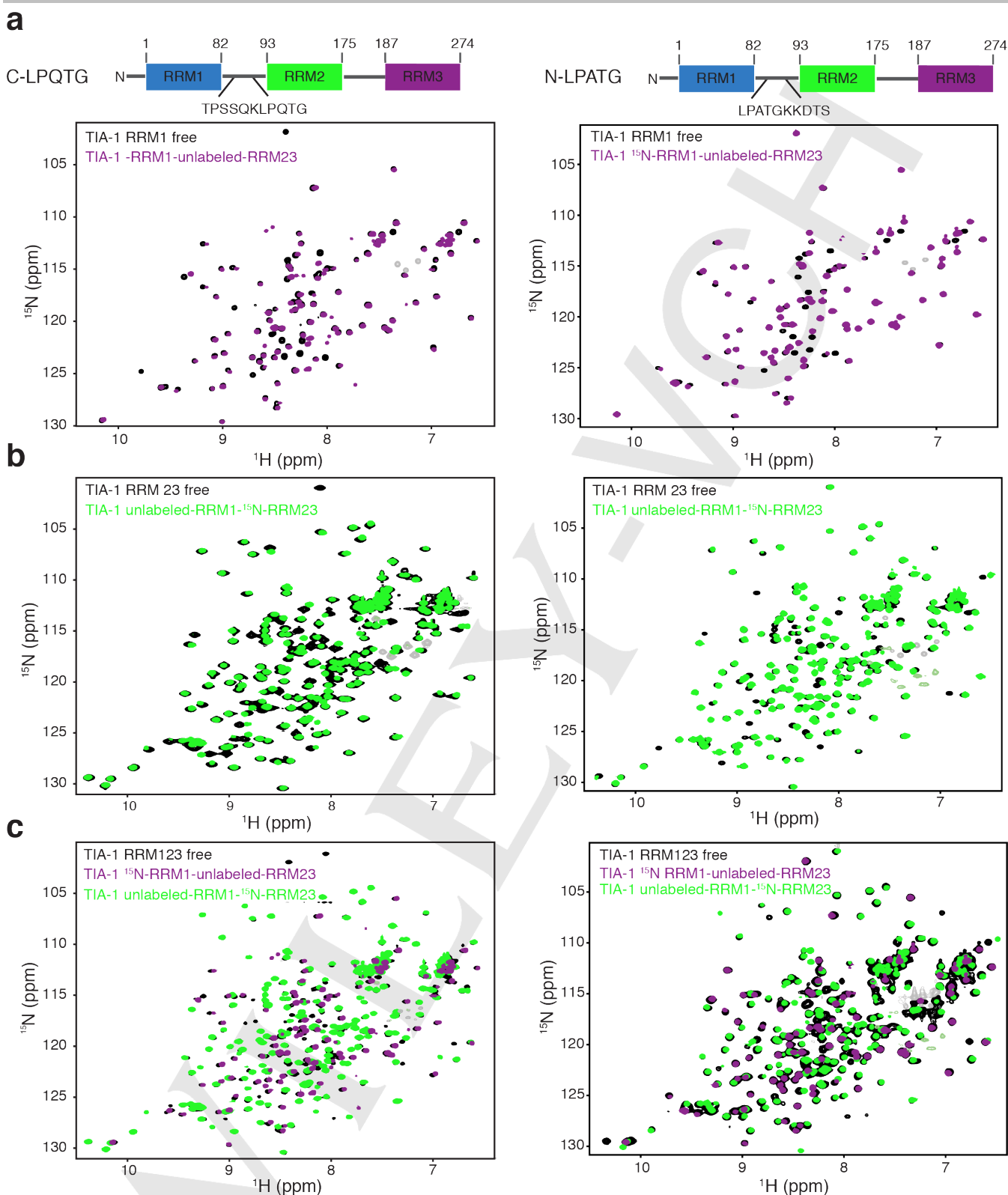


Figure S1. Overlay of ^1H , ^{15}N HSQC NMR spectra of different TIA-1 constructs. a) Overlay of segmentally labeled ^{15}N RRM1-RRM23 with uniformly labeled RRM1 single domain. In contrast to the RRM1 single domain both segmentally labeled samples contain RRM1-RRM2 linker residues to perform Sortase A-mediated ligation. b) Overlay of segmentally labeled RRM1- ^{15}N RRM23 and uniformly labeled tandem RRM23 construct. c) Overlay of both segmentally labeled spectra and uniformly ^{15}N labeled wild type TIA-1 RRM123. The almost identical chemical shifts of signals in the globular domains show that the Sortase A-ligation site residues do not affect the overall conformation. Additional signals are from linker residues which we had to mutate to ensure Sortase A recognition.

SUPPORTING INFORMATION

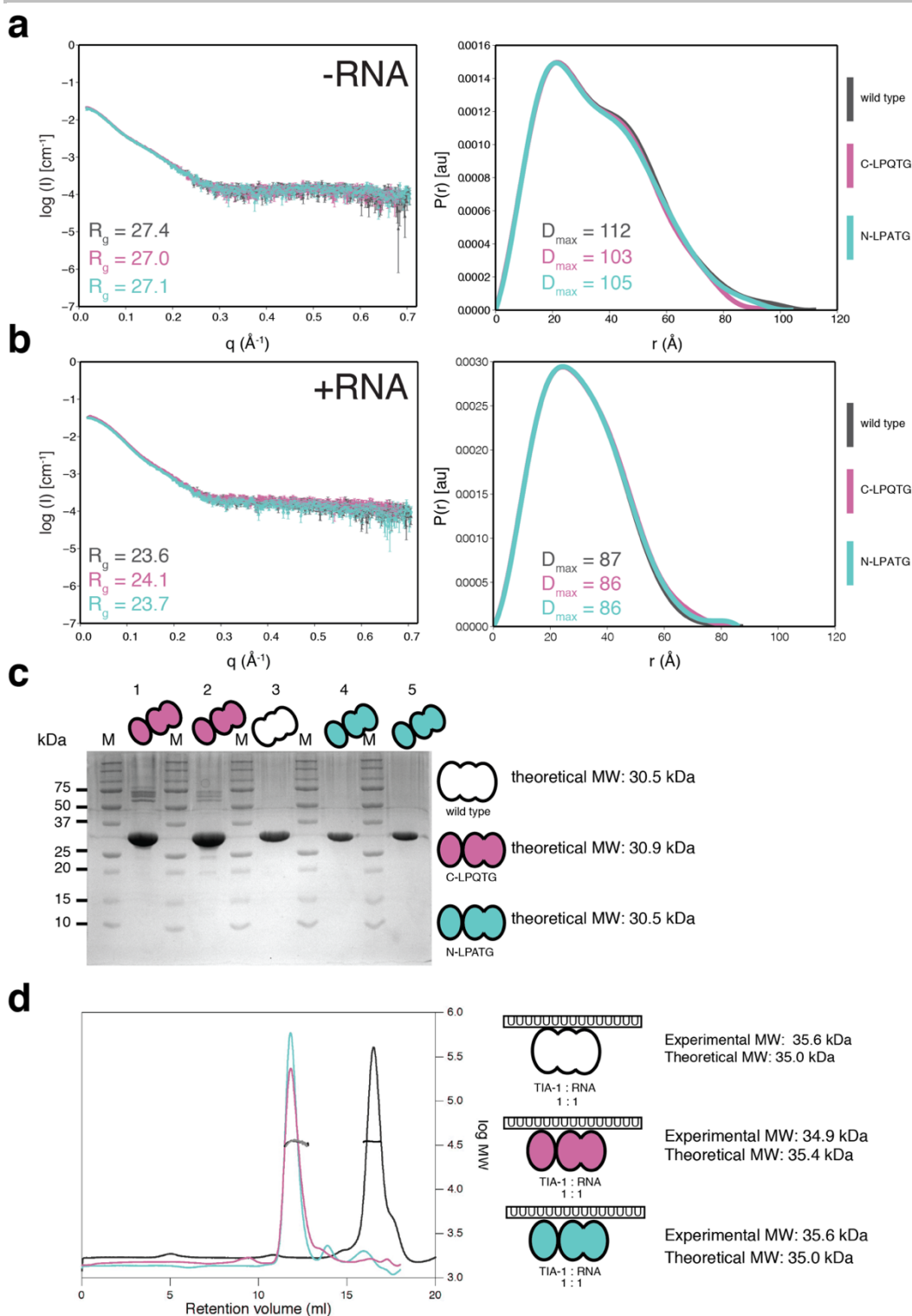


Figure S2. Quality assessment of all three constructs. Small-angle X-ray scattering for all three different constructs in the free form a) and bound to U15 b). The curves are deposited on SASBDB with the following IDs: wild type free (SASDCF3) and bound to U15 (SASDCC3), C-LPQTG free (SASDCD3) and bound to U15 (SASDCE3) and N-LPATG free (SASDCG3) and bound to U15 (SASDCH3). The scattering curves are shown on the left-hand side and the pairwise distribution functions on the right-hand side. The R_g and D_{max} values for each sample are given in the plots. c) SDS gel of the 3 different TIA-1 constructs. The cartoon above the gel indicates which construct is loaded in the corresponding line. The numbers on top correspond to the different labeling of the samples loaded. 1) ^{15}N RRM1-RRM23, 2) RRM1- ^{15}N RRM23, 3) wild type RRM123, 4) RRM1- ^{15}N RRM23, 5) ^{15}N RRM1 – RRM23. The theoretical MW of each construct is given on the right-hand side of the gel picture. The segmental labeled samples were taken directly after NMR measurements. All samples ran at the same height confirming the ligation success and the similarity to the wild type. The differences in the band size are because different volumes were loaded onto the gel (7 μl for samples 1 and 2 and 4 μl for samples 3 – 5) d) Determination of the molecular weight of TIA-1 RRM123 in complex with U15 RNA using size exclusion chromatography in combination with static light scattering. The wild type sample (black and dark grey) was run on a Superdex 200 column, the two segmentally labeled samples, C-LPQTG (magenta and black) and N-LPATG (cyan and light grey) on Superdex 75. The refractive index (shown) and right angle light scattering signals were used to calculate the molecular weights of 35.6, 34.9 and 35.6 kDa, respectively.

SUPPORTING INFORMATION

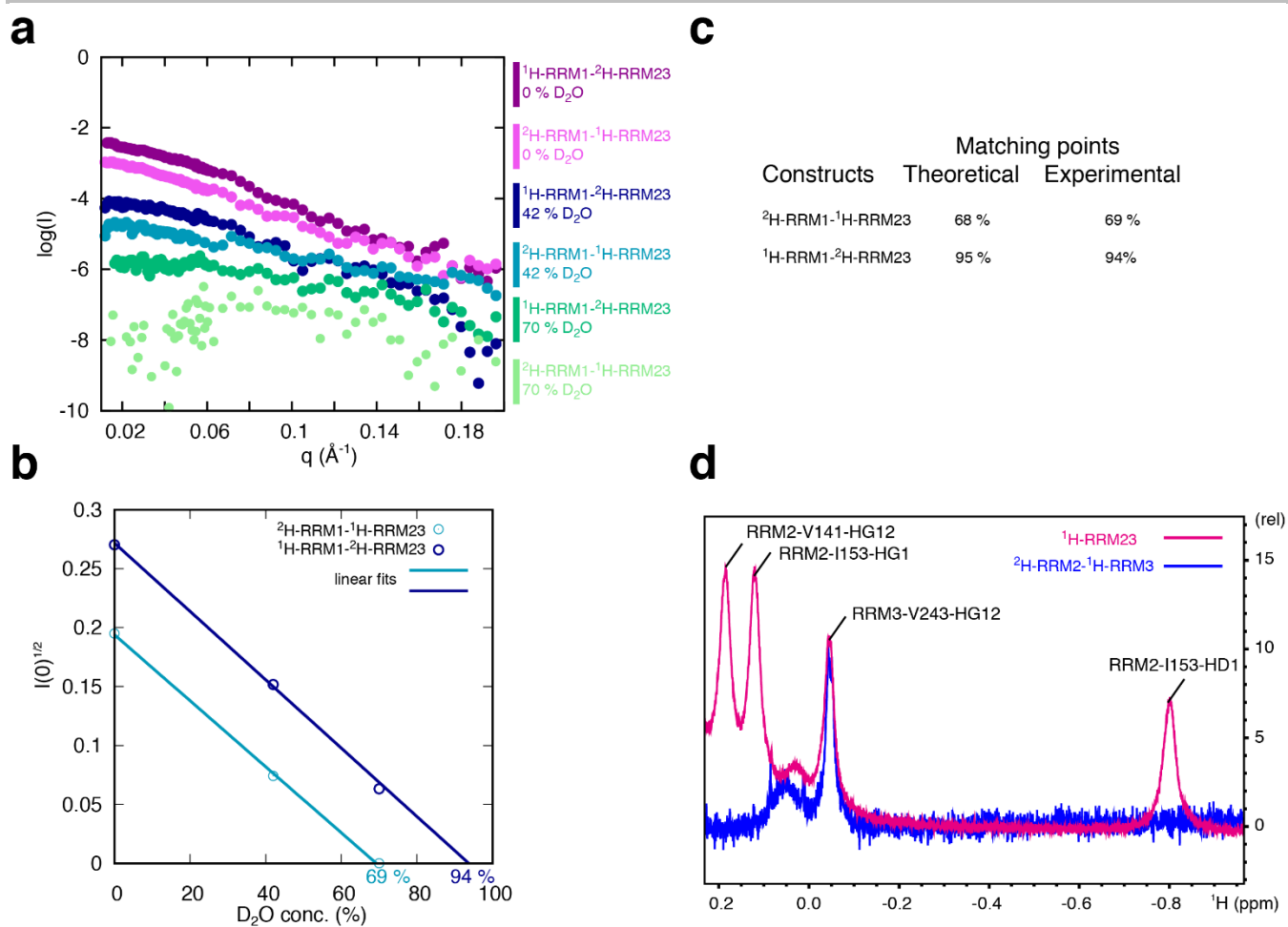


Figure S3. Assessment of the deuteration level of segmentally labeled protein samples. a) Scattering densities of all RNA bound samples, including 70 % D₂O. b) From these, $I(0)$ was derived and their square-root plotted versus the D₂O concentration of the sample solution. From the linear fit, the matching point for each construct is calculated to be 69 % for $^2\text{H-RRM1-}^1\text{H-RRM23}$ and 94 % for $^1\text{H-RRM1-}^2\text{H-RRM23}$, respectively. c) This matches the theoretical matching point with a deviation of 1 %. d) $^1\text{H-}^1\text{D}$ NMR of fully protonated RRM23 and segmentally perdeuterated $^2\text{H-RRM2-}^1\text{H-RRM3}$. The absence of methyl proton peaks belonging to RRM2 but not RRM3 indicates perdeuteration of RRM2.

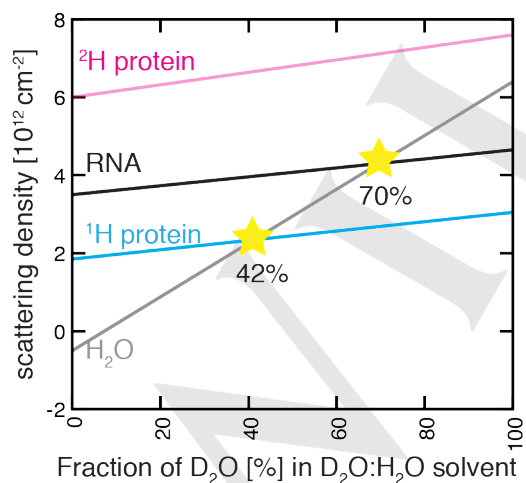


Figure S4. Scattering densities as a function of D₂O concentration in aqueous solvents for protonated and deuterated proteins as well as RNA (according to Jacrot^[30]). Contrast match points for each component are indicated by a yellow star.

SUPPORTING INFORMATION

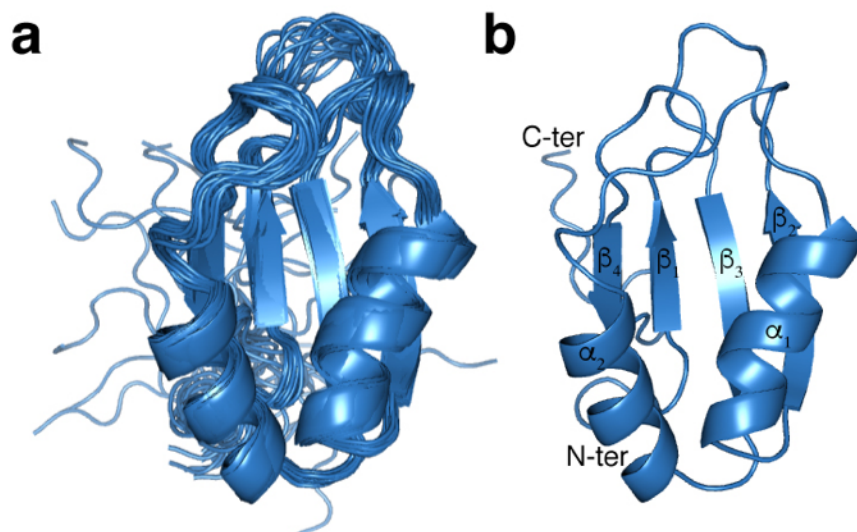


Figure S5. Solution NMR structure of TIA-1 RRM1 (PDB ID: 5O2V). a) Twenty lowest energy structures after water refinement are shown here. The structure is well converged with the formation of secondary structures except for N and C terminal regions which are flexible. b) Structure of a single lowest energy structure after water refinement is shown for clarity. RRM1 adopts a typical RRM fold with four β -sheets covered on one side by two α -helices.

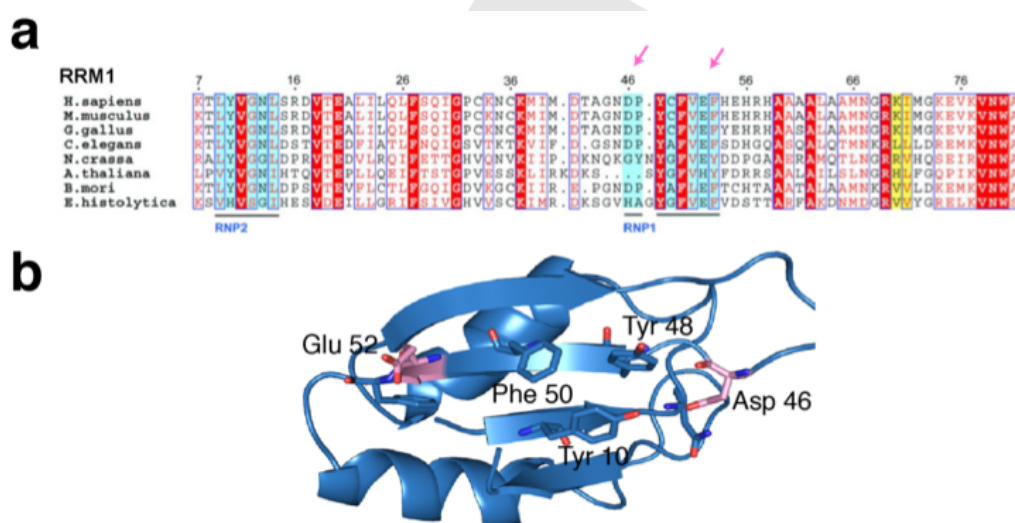


Figure S6. Structure analysis of TIA-1 RRM1. a) Sequence alignment of the TIA-1 RRM1 domain from different organisms is shown. Residues from the RNP1 and RNP2 are underlined and the negatively charged residues in the RNP1 are marked by pink arrows. b) The RNP1 and RNP2 residues are shown on the NMR structure of RRM1. The negatively charged residues are shown in pink.

SUPPORTING INFORMATION

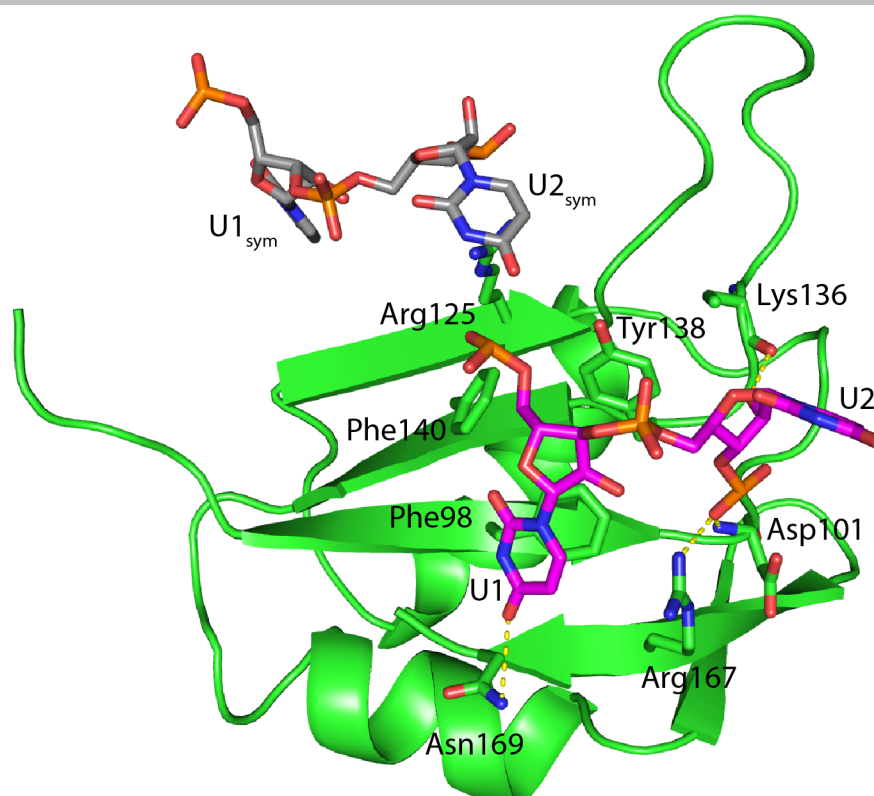


Figure S7. Crystal structure of TIA-1 RRM2 in complex with RNA (PDB ID: 5O3J). The hydrogen bonds are shown with yellow dotted lines. The residues of RRM2 interacting with RNA are labeled. The RNA from the unit cell is shown in magenta and the uridine bases are labeled U1 and U2 and the RNA from the symmetry mate is shown in grey and the bases are shown with U1_{sym} and U2_{sym}.

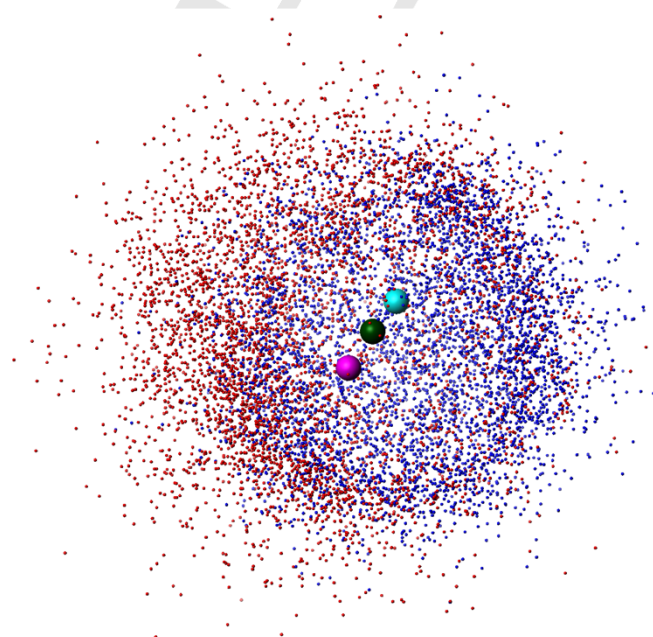


Figure S8. Conformation space and statistics of structure calculations. The large green ball is a C_α atom of RRM2 closest to the center-of-mass superimposed over all 5000 structures, whereas the pink and cyan ball are the C- and N-terminus, respectively. The small blue balls are the C_α atoms of RRM1 closest to its center-of-mass of all 5000 structures. The same is valid for RRM3 (red balls). This illustrates that the 5000 structures cover a large conformational space.

SUPPORTING INFORMATION

Table S1 Small-angle X-ray scattering statistic according to Jacques et al.^[31]

Data collection	Wild type free	C-LPQTG seg. labeled free	N-LPATG seg. labeled free	Wild type bound to U15	C-LPQTG seg. labeled bound to U15	N-LPATG seg. labeled bound to U15
Instrument	Rigaku BIOSAXS1000	Rigaku BIOSAXS1000	Rigaku BIOSAXS1000	Rigaku BIOSAXS1000	Rigaku BIOSAXS1000	Rigaku BIOSAXS1000
Beam geometry	point	point	point	point	point	point
Wavelength (Å)	1.542	1.542	1.542	1.542	1.542	1.542
q range (Å ⁻¹)	0.0094 - 0.704	0.0094 - 0.704	0.0094 - 0.704	0.0094 - 0.704	0.0094 - 0.704	0.0094 - 0.704
Exposure time (sec)	7200	7200	7200	7200	7200	7200
Concentration range (mg ml ⁻¹)	1.0 - 5.0	1.0 - 5.0	1.0 - 5.0	1.0 - 5.0	1.0 - 5.0	1.0 - 5.0
Temperature (K)	293	293	293	293	293	293
Structural parameters						
R _g (Å) from P(r)	28.9 ± 0.4	27.8 ± 0.4	28.5 ± 0.3	23.7 ± 0.2	24.2 ± 0.2	24.2 ± 0.2
I(0) (cm ⁻¹) from Guinier	0.023 ± 0.0004	0.023 ± 0.0002	0.022 ± 0.0003	0.036 ± 0.0002	0.038 ± 0.0002	0.034 ± 0.0003
R _g (Å) from Guinier	27.4 ± 0.5	27.0 ± 0.5	27.1 ± 0.6	23.6 ± 0.3	24.1 ± 0.2	23.7 ± 0.2
D _{max} (Å)	112	103	105	87	86	86
Porod volume estimated (Å ³)	38000	38000	37000	39000	40000	40000
Molecular-mass determination						
Molecular mass from Porod Volume (kDa)	29.8 ^a	30.7 ^a	30.3 ^a	-	-	-
Molecular mass from I(0) (kDa)	29.9 ^b	29.9 ^b	28.6 ^b	46.8 ^{b,c}	49.4 ^{b,c}	44.2 ^{b,c}
Theoretical mass from sequence (kDa)	30.5	30.9	30.5	35.0	35.4	35.0
Software employed						
Primary data reduction	SAXSLab (v 3.0.2)	SAXSLab (v 3.0.2)	SAXSLab (v 3.0.2)	SAXSLab (v 3.0.2)	SAXSLab (v 3.0.2)	SAXSLab (v 3.0.2)
Data processing	PRIMUS	PRIMUS	PRIMUS	PRIMUS	PRIMUS	PRIMUS

[a] The molecular mass of each unbound sample was calculated from the Porod Volume using the software package SAXS MoW2.^[32], [b] The molecular mass was calculated from the absolute calibrated scattering curves with a lysozyme sample as standard. [c] The experimental values of the molecular mass of the complex are higher than the theoretical one. This fact can be explained by the higher electronic scattering contrast of the bound RNA with respect to the protein part.

SUPPORTING INFORMATION

Table S2 Small-angle neutron scattering statistic according to Jacques et al.^[31]

Data collection	¹ H-RRM1- ² H-RRM23 0% D ₂ O	² H-RRM1- ¹ H-RRM23 0% D ₂ O	¹ H-RRM1- ² H-RRM23 42% D ₂ O	² H-RRM1- ¹ H-RRM23 42% D ₂ O	¹ H-RRM1- ² H-RRM23 0% D ₂ O + RNA	² H-RRM1- ¹ H-RRM23 0% D ₂ O + RNA	¹ H-RRM1- ² H-RRM23 42% D ₂ O + RNA	² H-RRM1- ¹ H-RRM23 42% D ₂ O + RNA
Instrument	KWS-1	KWS-1	KWS-1	KWS-1	KWS-1	KWS-1	KWS-1	KWS-1
Beam geometry	Pin-hole	Pin-hole	Pin-hole	Pin-hole	Pin-hole	Pin-hole	Pin-hole	Pin-hole
Wavelength (Å)	4.72	4.72	4.72	4.72	4.72	4.72	4.72	4.72
q range (Å ⁻¹)	0.0007 – 0.5	0.0007 – 0.5	0.0007 – 0.5	0.0007 – 0.5	0.0007 – 0.5	0.0007 – 0.5	0.0007 – 0.5	0.0007 – 0.5
Exposure time (min)	10-15 (2 m), 90-120 (8 m)	10-15 (2 m), 90-120 (8 m)	10-15 (2 m), 90-120 (8 m)	10-15 (2 m), 90-120 (8 m)	10-15 (2 m), 90-120 (8 m)	10-15 (2 m), 90-120 (8 m)	10-15 (2 m), 90-120 (8 m)	10-15 (2 m), 90-120 (8 m)
Concentration (mg ml ⁻¹)	5.0	5.0	5.0	5.0	5.0	5.0	5.0	5.0
Temperature (K)	293	293	293	293	293	293	293	293
Structural parameters								
R _g (Å) from P(r)	28.7 ± 0.1	28.9 ± 0.0	23.3 ± 0.02	15.8 ± 0.0	25.5 ± 0.1	25.2 ± 0.1	23.3 ± 0.0	18.0 ± 0.0
R _g (Å) from Guinier	28.6 ± 0.5	27.8 ± 0.7	24.1 ± 1.6	16.3 ± 0.5	25.4 ± 0.1	25.1 ± 0.1	23.5 ± 0.0	18.1 ± 0.5
D _{max} (Å)	105	104	81	48	83	84	73	50
Porod volume estimated (Å ³)	33000	34000	24000	17000	36000	34000	28000	9000
Software employed								
Primary data reduction	QtiKWS	QtiKWS	QtiKWS	QtiKWS	QtiKWS	QtiKWS	QtiKWS	QtiKWS
Data processing	PRIMUS	PRIMUS	PRIMUS	PRIMUS	PRIMUS	PRIMUS	PRIMUS	PRIMUS

SUPPORTING INFORMATION

Table S3 Structural statistics for TIA-1 RRM1.

Structural characteristics for TIA-1 RRM1	
Structure calculation restraints	
Distance restraints	
Total NOEs	981
Sequential ($ i-j = 1$)	564
Medium-range ($ i-j \leq 4$)	125
Long-range ($ i-j > 4$)	292
Hydrogen bonds	29
Dihedral restraints ($\phi+\psi$)	138
Quality analysis	
Restrains violations (mean \pm s.d.)	
Distance restraints (Å)	0.054 \pm 0.021
Dihedral angle restraints ($^\circ$)	0.38 \pm 0.00
Deviation from idealized geometry	
Bond length (Å)	1.024 \pm 0.001
Bond angles ($^\circ$)	0.329 \pm 0.006
Improper dihedral distribution ($^\circ$)	0.412 \pm 0.017
Average pairwise r.m.s. deviation (Å) ^a	
Heavy	1.13 \pm 0.1
Backbone	0.49 \pm 0.08
Ramachandran values (%) ^{a,b}	
Most favored regions	91.6
Allowed regions	7.4
Generously allowed regions	0.2
Disallowed regions	0.8
WhatIf analysis ^{a,c}	
First generation packing	2.278 \pm 0.0.889
Second generation packing	5.655 \pm 1.711
Ramachandran plot appearance	-2.341 \pm 0.589
Chi-1/Chi-2 rotamer normality	-2.025 \pm 0.744
Backbone conformation	0.653 \pm 0.421

[a] For residues 9–40, 47–81, [b] With Procheck^[14] [c] Analyzed by iCING^[13]. Structure Z-scores, a positive number is better than average.

SUPPORTING INFORMATION

Table S4 Crystal structure statistics for TIA-1 RRM2 in complex with RNA.

Wavelength (Å)		0.99
Resolution range (Å)	35.02 - 2.97	(3.076 - 2.97)
Space group		P 65
Unit cell (Å)	44.31 44.31 85.72	90 90 120
Total reflections		15406 (1561)
Unique reflections		1980 (192)
Multiplicity		7.8 (8.0)
Completeness (%)		0.98 (1.00)
Mean I/sigma(I)		15.34 (2.10)
Wilson B-factor		82.10
R-merge		0.08676 (0.6048)
R-meas		0.09314 (0.6481)
CC1/2		0.998 (0.939)
CC*		0.999 (0.984)
Reflections used in refinement		1952 (194)
Reflections used for R-free		98 (10)
R-work		0.2514 (0.2551)
R-free		0.3112 (0.2497)
Number of non-hydrogen atoms		643
macromolecules		643
RMS(bonds)		0.007
RMS(angles)		0.91
Ramachandran favored (%)		96
Ramachandran allowed (%)		2.6
Ramachandran outliers (%)		1.3
Rotamer outliers (%)		1.9
Average B-factor		89.71
macromolecules		89.71

Statistics for the last shell are shown in parenthesis.

SUPPORTING INFORMATION

Table S5 Statistics of structure calculations for TIA-1 RRM123. Each filter step reduces not only the number of structures but also decrease the deviation of the structural ensemble, regarding the radius of gyration and the distances between the domains, as well as the angle. Interestingly, the distance between RRM1 and RRM2 or RRM1 and RRM3 has a larger spread than the distance between RRM2 and RRM3, indicating that RRM1 is further extended and not in contact with RNA, which otherwise compacts RRM2 and RRM3.

	R_g	Distance RRM1- RRM2 (Å)	Distance RRM1- RRM3 (Å)	Distance RRM2- RRM3 (Å)	Angle RRM1-2-3
All 5000 structures					
Run 1	23.3 ± 2.6	31.2 ± 7.5	40.3 ± 12.1	31.7 ± 7.6	82.6 ± 34.4
Run 2	23.3 ± 2.7	31.3 ± 7.7	40.0 ± 12.3	31.7 ± 7.8	81.9 ± 35.1
Run 1+2	23.3 ± 2.6	31.2 ± 7.6	40.2 ± 12.2	31.7 ± 7.7	82.2 ± 34.7
After SAXS filter					
Run 1	23.8 ± 1.1	32.8 ± 5.2	44.7 ± 7.6	31.0 ± 4.0	92.8 ± 28.0
Run 2	23.9 ± 1.0	32.6 ± 6.1	45.1 ± 7.6	31.0 ± 4.1	95.2 ± 29.6
Run 1+2	23.9 ± 1.0	32.7 ± 5.6	44.9 ± 7.6	31.0 ± 4.0	94.0 ± 28.8
After SANS filter					
Run 1	25.9 ± 0.3	35.6 ± 3.2	55.3 ± 1.4	34.1 ± 2.9	106.8 ± 15.0
Run 2	25.3 ± 0.3	37.9 ± 5.2	48.8 ± 3.9	34.0 ± 2.1	86.3 ± 15.5
Run 1+2	25.6 ± 0.5	36.7 ± 4.2	52.1 ± 4.4	34.1 ± 2.4	96.6 ± 18.0

SUPPORTING INFORMATION

References

- [1] L. Freiburger, M. Sonntag, J. Hennig, J. Li, P. Zou, M. Sattler, *Journal of biomolecular NMR* **2015**, *63*, 1-8.
- [2] F. Delaglio, S. Grzesiek, G. W. Vuister, G. Zhu, J. Pfeifer, A. Bax, *Journal of biomolecular NMR* **1995**, *6*, 277-293.
- [3] T. D. a. K. Goddard, D.G., *University of California, San Francisco*.
- [4] B. A. Johnson, R. A. Blevins, *J. Biomol. NMR* **1994**, *4*, 603-614.
- [5] M. Sattler, J. Schleucher, C. Griesinger, *Progress in Nuclear Magnetic Resonance Spectroscopy* **1999**, *34*, 93-158.
- [6] R. L. J. Keller, *The Computer Aided Resonance Assignment Tutorial*, 1st ed., CANTINA Verlag, **2004**.
- [7] S. Grzesiek, A. Bax, *J. Biomol. NMR* **1993**, *3*, 185-204.
- [8] T. Yamazaki, J. D. Forman-Kay, L. E. Kay, *J. Am. Chem. Soc.* **1993**, *115*, 11054-11055.
- [9] W. F. Vranken, W. Boucher, T. J. Stevens, R. H. Fogh, A. Pajon, M. Llinas, E. L. Ulrich, J. L. Markley, J. Ionides, E. D. Laue, *Proteins* **2005**, *59*, 687-696.
- [10] P. Guntert, *Methods Mol Biol* **2004**, *278*, 353-378.
- [11] Y. Shen, F. Delaglio, G. Cornilescu, A. Bax, *J. Biomol. NMR* **2009**, *44*, 213-223.
- [12] aJ. P. Linge, M. Habeck, W. Rieping, M. Nilges, *Bioinformatics* **2003**, *19*, 315-316; bJ. P. Linge, M. A. Williams, C. A. E. M. Spronk, A. M. J. J. Bonvin, M. Nilges, *Proteins: Structure, Function, and Bioinformatics* **2003**, *50*, 496-506.
- [13] J. F. Doreleijers, A. W. Sousa da Silva, E. Krieger, S. B. Nabuurs, C. A. Spronk, T. J. Stevens, W. F. Vranken, G. Vriend, G. W. Vuister, *Journal of biomolecular NMR* **2012**, *54*, 267-283.
- [14] R. A. Laskowski, J. A. Rullmann, M. W. MacArthur, R. Kaptein, J. M. Thornton, *Journal of biomolecular NMR* **1996**, *8*, 477-486.
- [15] G. Vriend, C. Sander, *Journal of Applied Crystallography* **1993**, *26*, 47-60.
- [16] H. M.-L. Zentrum, *Journal of large-scale research facilities* **2015**, *1*.
- [17] M. D. Lixin Fan, Scott Bendle, Nick Grupido and Jan Ilavsky, *Journal of Physics: Conference Series* **2010**, *247*.
- [18] M. V. Petoukhov, D. Franke, A. V. Shkumatov, G. Tria, A. G. Kikhney, M. Gajda, C. Gorba, H. D. T. Mertens, P. V. Konarev, D. I. Svergun, *Journal of Applied Crystallography* **2012**, *45*, 342-350.
- [19] P. V. Konarev, V. V. Volkov, A. V. Sokolova, M. H. J. Koch, D. I. Svergun, *Journal of Applied Crystallography* **2003**, *36*, 1277-1282.
- [20] D. Svergun, *Journal of Applied Crystallography* **1992**, *25*, 495-503.
- [21] A. T. Brunger, *Nat Protoc* **2007**, *2*, 2728-2733.
- [22] M. Nilges, *Journal of molecular biology* **1995**, *245*, 645-660.
- [23] B. Simon, T. Madl, C. D. Mackereth, M. Nilges, M. Sattler, *Angewandte Chemie* **2010**, *49*, 1967-1970.
- [24] A. Lapinaite, B. Simon, L. Skjaerven, M. Rakwalska-Bange, F. Gabel, T. Carlomagno, *Nature* **2013**, *502*, 519-523.
- [25] W. Kabsch, *Acta Crystallogr D Biol Crystallogr* **2010**, *66*, 125-132.
- [26] A. J. McCoy, R. W. Grosse-Kunstleve, P. D. Adams, M. D. Winn, L. C. Storoni, R. J. Read, *J Appl Crystallogr* **2007**, *40*, 658-674.
- [27] M. D. Winn, C. C. Ballard, K. D. Cowtan, E. J. Dodson, P. Emsley, P. R. Evans, R. M. Keegan, E. B. Krissinel, A. G. Leslie, A. McCoy, S. J. McNicholas, G. N. Murshudov, N. S. Pannu, E. A. Potterton, H. R. Powell, R. J. Read, A. Vagin, K. S. Wilson, *Acta Crystallogr D Biol Crystallogr* **2011**, *67*, 235-242.
- [28] P. Emsley, K. Cowtan, *Acta Crystallogr D Biol Crystallogr* **2004**, *60*, 2126-2132.
- [29] G. N. Murshudov, A. A. Vagin, E. J. Dodson, *Acta Crystallogr D Biol Crystallogr* **1997**, *53*, 240-255.
- [30] B. Jacrot, *Reports on progress in physics* **1976**, *39*, 911.
- [31] D. A. Jacques, J. M. Guss, D. I. Svergun, J. Trehwella, *Acta Crystallogr D Biol Crystallogr* **2012**, *68*, 620-626.
- [32] H. Fischer, M. de Oliveira Neto, H. B. Napolitano, I. Polikarpov, A. F. Craievich, *Journal of Applied Crystallography* **2010**, *43*, 101-109.